ANL/CHM/CP-100372

(28th Symposium (International) on Combustion, Dec. 15, 1999)

RECEIVED
JAN 18 2000
OSTI

INITIATION IN H_2/O_2: RATE CONSTANTS FOR $H_2 + O_2 \rightarrow H + HO_2$ AT HIGH TEMPERATURE

by

J. V. Michael*, J. W. Sutherland#, L. B. Harding*, and A. F. Wagner*

Chemistry Division, Argonne National Laboratory, Argonne, IL 60439, USA

Corresponding Author: **Dr. J. V. Michael**
D-193, Bldg. 200
Argonne National Laboratory
Argonne, IL 60439, USA
Phone: (630) 252-3171, Fax: (630) 252-4470
E-mail: Michael@anlchm.chm.anl.gov

Presentation Mode:	Oral Presentation
Preferred Publication:	Proceedings
Category:	Reaction Kinetics of Combustion

	Text	Reference	Tables	Figures	Total
Count	10 pages	48 citations	2 pages	3 pages	
Equiv. Words	3177	952	400	600	5129

The submitted manuscript has been created by the University of Chicago as Operator of Argonne National Laboratory ("Argonne") under Contract No. W-31-109-ENG-38 with the U.S. Department of Energy. The U.S. Government retains for itself, and others acting on its behalf, a paid-up, nonexclusive, irrevocable worldwide license in said article to reproduce, prepare derivative works, distribute copies to the public, and perform publicly and display publicly, by or on behalf of the Government.

#Present address: Guest Scientist, Department of Applied Science, Brookhaven National Laboratory, Upton, NY 11973

This work was supported by the U. S. Department of Energy, Office of Basic Energy Sciences, Division of Chemical Sciences, under Contract No. W-31-109-Eng-38.

DISCLAIMER

This report was prepared as an account of work sponsored by an agency of the United States Government. Neither the United States Government nor any agency thereof, nor any of their employees, make any warranty, express or implied, or assumes any legal liability or responsibility for the accuracy, completeness, or usefulness of any information, apparatus, product, or process disclosed, or represents that its use would not infringe privately owned rights. Reference herein to any specific commercial product, process, or service by trade name, trademark, manufacturer, or otherwise does not necessarily constitute or imply its endorsement, recommendation, or favoring by the United States Government or any agency thereof. The views and opinions of authors expressed herein do not necessarily state or reflect those of the United States Government or any agency thereof.

DISCLAIMER

Portions of this document may be illegible in electronic image products. Images are produced from the best available original document.

Abstract

The reaction between H_2 and O_2 has been studied in a reflected shock tube apparatus between 1662-2097 K. O-atom atomic resonance absorption spectrometry (ARAS) was used to observe absolute $[O]_t$ under conditions of low $[H_2]_0$ so that most secondary reactions were negligible. Hence, the observed $[O]_t$ was the direct result of the rate controlling reaction between H_2 and O_2. Three different reactions were considered, but experimental and *ab initio* theoretical results both indicated that the process, $H_2 + O_2 \rightarrow H + HO_2$, is the only possible reaction. After rapid HO_2 dissociation, O-atoms are then instantaneously produced by $H + O_2 \rightarrow O + OH$. Using the *ab initio* result, conventional transition state theoretical calculations (CTST) with tunneling corrections give the expression: $k = 1.228 \times 10^{-18} T^{2.4328} \exp(-26926 \text{ K}/T)$ cm^3 $molecule^{-1}$ s^{-1}, applicable between 400 and 2300 K. This theoretical result agrees with the present experimental determinations and those at lower temperature, derived from earlier work on the reverse reaction.

Introduction

The branching chain oxidation of H_2 with O_2 is one of the most studied reactions in combustion. It was recognized very early that branching could only occur after some initiation process produces radical chain centers [1]. Over the years, five initiation reactions have been considered:

$$H_2 + O_2 \rightarrow H + HO_2, \tag{1}$$

$$H_2 + O_2 \rightarrow OH + OH, \tag{2}$$

$$H_2 + O_2 \rightarrow O + H_2O, \tag{3}$$

$$H_2 + M \rightarrow H + H + M, \tag{4}$$

and,

$$O_2 + M \rightarrow O + O + M. \tag{5}$$

Reactions (1) and (2) have been the preferred initiation processes since reaction (3) requires multiple bond rearrangement and both diatomic dissociation reactions, (4) and (5), require substantially higher energy [2]. Reaction (2) was almost always the choice in shock tube induction delay experiments [3-6] until ~1985, with the value from Ripley and Gardiner [3], $k_2 = 4.16 \times 10^{-12} \exp(-19605\ K/T)$ cm^3 $molecule^{-1}$ s^{-1}, being typical. However, later flow tube studies at room temperature [7,8] on the reverse of reaction (1), $H + HO_2, \rightarrow H_2 + O_2$, gave a rate constant of $k_{-1} = 6.7 \times 10^{-12}$ cm^3 $molecule^{-1}$ s^{-1} with at least an error of ±50%, essentially corroborating earlier values [9,10]. Using Janaf calculated equilibrium constants [11], Warnatz [12] then estimated rate constants for reaction (1) and suggested its importance as an initiation process. With derived 773 K results from Baldwin et al. [13] (i. e., $k_{-1} = 4.65 \times 10^{-11}$ cm^3 $molecule^{-1}$ s^{-1}), Tsang and Hampson [14] further refined the estimate, albeit with a large uncertainty, suggesting $k_1 = 2.4 \times 10^{-10} \exp(-28500\ K/T)$ cm^3 $molecule^{-1}$ s^{-1} for 300-800 K.

From the above discussion, it is clear that currently used values for initiation with reactions (1), (2), or (3) are based on a relatively small experimental database. In the present work, we have studied the $H_2 + O_2$ reaction with atomic resonance absorption spectrometry (ARAS) under low $[H_2]$ conditions using the reflected shock tube technique. Absolute rates of O-atom formation are measured during the initial stages of reaction under conditions where the rate of initiation is rate controlling and nearly chemically isolated. Previous ARAS studies [6,15,16] did not use a sufficiently high $[O_2]/[H_2]$ ratio to allow kinetic isolation of the initiation process. The difficulty in assessing initiation with ignitable quantities of H_2 and O_2 is well illustrated in the work of Pamidimukkala and Skinner [6] who finally conclude that thermal dissociation of impurities probably initiated the branching chain oxidation in their work. By contrast in the present work, $[H_2]$ is so small and impurity levels are so low that any observed atom formation must derive from a direct bimolecular reaction between H_2 and O_2.

Experimental

The present experiments were performed with previously described equipment [17], and, therefore, only a brief description of the system, along with those features unique to the current experimental procedures, will be presented here.

The apparatus consists of a 7-m (4-in. o.d.) 304 stainless steel tube separated from the He driver chamber by a 4 mil unscored 1100-H18 aluminum diaphragm. The tube was routinely pumped between experiments to less than 10^{-8} Torr by an Edwards Vacuum Products Model CR100P packaged pumping system. The velocity of the shock wave was measured with eight equally spaced pressure transducers (PCB Piezotronics, Inc., Model 113A21) mounted along the downstream part of the test section of the shock tube and recorded with a 4094C Nicolet digital oscilloscope. Temperature and density in the reflected shock wave regime were calculated from this velocity. This procedure, which includes corrections for boundary layer perturbations, has been fully described elsewhere [17,18]. The digital oscilloscope was triggered by pulses derived from the last velocity gauge signal. The photometer system was radially located 6 cm from the endplate. All optics were made from MgF_2. The resonance lamp beam intensity was measured by an EMR G14 solar blind photomultiplier tube and recorded with the oscilloscope.

The technique used for the detection of the transient O-atoms is atomic resonance absorption spectroscopy (ARAS). In earlier work [19], an O-atom curve-of-growth was determined using $X_{O_2} = 1 \times 10^{-3}$ in 1.8 Torr of purified grade He at 50 watts microwave power to give an effective lamp temperature of 490 K [20]. This curve-of-growth was slightly modified with the inclusion of additional data obtained in a later study [21]. The present experiments were carried out in exactly the same way as in this earlier study [21] except that H_2 was used as the reactant instead of CH_3. Following procedures discussed earlier [21], twenty-eight kinetics experiments were carried out between 1662 and 2097 K under the conditions shown in Table 1.

Gases: High purity He (99.995%), used as the driver gas, was from Air Products and Chemicals, Inc. Scientific grade Kr (99.999%), the diluent gas in reactant mixtures, was from Spectra Gases, Inc. In Kr, the ~10 ppm impurities (N_2 - 2 ppm, O_2 - 0.5 ppm, Ar - 2 ppm, CO_2 - 0.5 ppm, H_2 - 0.5 ppm, CH_4 - 0.5 ppm, H_2O - 0.5 ppm, Xe - 5 ppm, and CF_4 - 0.5 ppm) are all either inert or in sufficiently low concentration so as to not perturb O-atom profiles. Ultra-high purity grade He (99.999% from AGA Gases) was used for the resonance lamp. High purity O_2 (99.995%) for the atomic filter was from AGA Gases. Scientific grade O_2 (99.999%) and H_2 (99.9999%) for reaction mixtures, were obtained from MG Industries and were used without additional purification. Test gas mixtures were accurately prepared from pressure measurements using a Baratron capacitance manometer and were stored in an all glass vacuum line.

Results

With the relatively high levels of O_2 used in the present experiments, there is an observable absorption of the resonance light at 130 nm by molecular oxygen. Since this absorption is uniform over the O_2 bandwidth and $[O_2]$ does not significantly change during an experiment, any observed decrease in the transmitted light intensity without reactant H_2 reflects an increase in total density (due to vibrational relaxation of O_2) and/or O-atom formation from $O_2 + M \rightarrow 2O + M$ at high temperature. Hence, we carried out a limited set of O_2 dissociation experiments with the same $[O_2]$ that was used in the kinetics experiments. Under conditions where O-atom formation was negligible, density relaxation (generally <250 μs at $T > 1600$ K) was easily determined. The apparent absorbance due to the vibrational relaxation of O_2 was a small correction and was not strongly dependent on temperature. This correction was then point-by-point subtracted from the higher temperature runs where O-atoms were definitely formed from dissociation as reflected in a substantial strong increase in absorption. The corrected absorbance was then converted to $[O]_t$ with the previously determined curve-of-growth [21]. Using the expression, $k_d = R_0/2[O_2][M]$, where R_0 is the rate of formation of O-atoms (i. e., the slope from the experimental $[O]_t$ against t plots), values for k_d were determined. For $T > 2200$ K the results were within ±40% of those accurately determined previously by Jerig, Thielen, and Roth [24]. Hence, we have adopted their value in the kinetics model for the H_2/O_2 experiments. In the kinetics runs listed in Table 1, we similarly corrected for O_2 density relaxation by point-by-point subtraction. In general, the contribution of this correction was ~20%; i. e., 80% of the signal was due to chemical reaction with reactant H_2. After conversion to $[O]_t$ using the curve-of-growth [21], O-atom concentration profiles were determined, two of which are shown in Fig. 1. These experimental profiles were then compared to those generated by numerical integration of the reaction mechanism listed in Table 2.

Discussion

Experiment: $[O]_t$ profiles (0 to 1 ms) of the twenty-eight experiments in Table 1 were generally simulated over the concentration range, 0 to $\sim 1 \times 10^{13}$ atoms cm^{-3}, using the mechanism of Table 2. For the conditions shown, the only important reactions in the table are (1), (2), or (3), possibly followed by (6) through (9). In the initial stages of reaction, all radical-radical processes are negligibly slow as are the reactions, H and/or O + H_2O, both of which have high activation energies. H_2 dissociation, reaction (4), is also too slow for the small $[H_2]$ employed. However, O_2 dissociation [24] can significantly contribute to O-atom formation at $T > 2100$ K, and therefore, no experiments above this temperature were included in the database. Under all experimental conditions, reactions (6) and (7) are effectively instantaneous leaving only reactions (8) and (9) contributing to the time dependence of $[O]_t$. Hence, fitting is dependent only on the values of the rate constants for (1), (2), or (3) and by (8) and (9), both of which are well known over the present T-range [25].

Even though most of the reactions are relatively unimportant, the entire set of reactions in Table 2 was used to simulate $[O]_t$. Figure 1 shows two such profiles. The solid or dashed lines are simulations under the separate assumptions that either reaction (1) or (2) initiates the reaction. In both cases, the values resulted from iterative fits, and doubling or halving the rate constants for either process results in values of $[O]_t$ at 1 ms that are about twice or one-half of those from the best fits. Given the substantial experimental error in absolute [O] (i. e., ~±15%)[21], the fits give rate constant values with an estimated accuracy of ~±20%. Inspection of Fig. 1 shows that either (1) or (2) (or possibly both) could account for the results, and, therefore, we determined rate constant values for the entire set of experiments in Table 1 using either reaction as the initiation process. If reaction (2) is presumed to be the initiation process then the derived rate constants follow the Arrhenius expression: $k_2 = 1.01 \times 10^{-8} \exp(-33056\ K/T)\ cm^3\ molecule^{-1}\ s^{-1}$ whereas, with reaction (1), the value is:

$$k_1 = 1.50 \times 10^{-11} \exp(-22905\ K/T)\ cm^3\ molecule^{-1}\ s^{-1}. \qquad (6)$$

for $1662 \leq T \leq 2097$ K. Since the data are obtainable over such a limited T-range, deciding between (1) and (2) is impossible from just these results alone. Considering reaction (3), if this were the initiation process then the only important reaction would be (3) alone, and, in this case the values for k_3 would be ~2 times Eq. 6. A choice might be possible by examining A-factors and activation energies from the three analyses. If (2) or (3) were operative then one would expect low A-factors (i. e., $\sim 10^{-12}\ cm^3\ molecule^{-1}\ s^{-1}$) for four-center or tight transition states, respectively [27], but much higher values, $A_2 \sim 1 \times 10^{-8}$ or $A_3 \sim 3 \times 10^{-11}\ cm^3\ molecule^{-1}\ s^{-1}$, are required to explain the data. Moreover, it is also worth noting that reaction (2) violates Woodward-Hoffman rules. Hence, from the experimental evidence, we consider reaction (1), summarized in Eq. 6, as the most likely initiation process. Eq. 6 gives values that agree well within a factor of 2 with those of Tsang and Hampson [14] over the experimental T-range, 1600-2100 K. The values from Koike [16] range from 3 to 20 times higher, and those from Skinner et al. [28] are substantially lower than those calculated from Eq. 6. Hence, it is our considered conclusion that reaction (1) is the only viable process responsible for initiation in the H_2/O_2 system. In the theoretical discussion to follow, this conclusion will be further assessed in terms of *ab initio* determinations of potential energy surfaces for both processes. Subsequently conventional transition state theoretical (CTST) estimates of the thermal rate behavior will be presented and compared with experiment.

Theory: The electronic structure calculations focus on locating transition states for reactions (1) to (3). Hence, preliminary searches were made by employing low-levels of theory which allow large volumes of configuration space to be explored, and then, when a given transition state is located, the structure is re-optimized at higher and more accurate levels of theory. All calculations employ the Dunning [29-31] correlation-consistent basis sets. The preliminary searches were made using the polarized valence double zeta basis set (cc-pvdz) and the critical stationary points were re-examined using the polarized quadruple zeta (cc-pvqz) basis set. Searches were carried out with both coupled cluster, CCSD(T) [32], and complete active space, self-consistent field, CASSCF [33,34] calculations. The CCSD(T) method is the most accurate, single-reference, *ab initio* method currently available. The CASSCF calculations were done to check on the possibility of transition state structures located in regions not well described by single-reference wavefunctions. In the CASSCF calculations reported here, all valence electrons were taken as active except the oxygen 2s electrons. The active space thus consists of 8 orbitals and 10 electrons (1512 configuration state functions). All calculations were carried out using the MOLPRO package of codes [35].

A transition state for reaction (1) was readily located. At the highest level of theory used (i. e., CCSD(T)/cc-pvqz), the structure is as follows: R_{OO}=1.30Å, R_{OHa}=1.05Å, R_{OHb}=2.24Å, HaOO$\angle$=107.1°, and HbOO$\angle$=107.7°. As expected for an endothermic reaction, the transition state is very "late" with an OH bond extension of only 0.08Å, relative to HO_2 and an HH bond extension of 0.45Å, relative to H_2. The calculated, in-plane, harmonic frequencies are 1717, 1374, 1169, 321, and 1825i cm^{-1}. These can be compared to calculated frequencies for $H_2 + O_2$ of 4403 and 1600 cm^{-1} and, for HO_2, of 3672, 1441, and

1142 cm^{-1}. For the out-of-plane bending mode of the transition state it was not possible to do calculations at the CCSD(T)/cc-pvqz level. For this mode we use the result of a CCSD(T)/cc-pvdz calculation, namely, 681 cm^{-1}.

The calculated barrier, without zero point corrections, is 57.8 kcal $mole^{-1}$. For comparison, calculations with cc-pvdz and cc-pvtz basis sets give barriers of 60.2 and 58.3 kcal $mole^{-1}$. Most of the decrease in barrier height with increasing basis set size correlates with a decreasing endothermicity; i. e., the small reverse barrier is less sensitive to the level of theory. The calculated reverse barriers are 2.9, 2.6, and 2.7 kcal $mole^{-1}$ using cc-pvdz, cc-pvtz and cc-pvqz basis sets, respectively.

Regarding the cc-pvqz zero point corrected endothermicity for reaction (1), 55.4 kcal $mole^{-1}$ is obtained, and this value is in excellent agreement with recent measurements by Litorja and Ruscic [36], 55.7±0.8 kcal $mole^{-1}$. This new endothermicity [36] is 2.8 kcal $mole^{-1}$ higher than used by Janaf [11], and therefore the Janaf estimated equilibrium constants are ~1.64 to100 times larger than implied by Litorja and Ruscic from 2500 down to 300 K. With the harmonic oscillator approximation, K_{eq} for reaction (1) can be calculated using these experimental results [36], giving to within ±3%,

$$K_{eq} = 0.2021\ T^{0.3455} \exp(-27656\ K/T), \tag{7}$$

between 300 and 2500 K. K_{eq} can also be calculated from the present theory, and there is only a few percent difference between theory and experiment, corroborating the accuracy of the present *ab initio* results.

Extensive searches (i. e., ~10^5 points) were also made for the transition states of reactions (2) and (3). The searches were carried out at both the CCSD(T)/cc-pvdz and CASSCF/cc-pvdz levels. No transition state for either reaction could be found. While the existence of a transition state connecting any two minima on a multi-dimensional potential surface is guaranteed, the existence of a *direct* transition state is not. Previous calculations

[37] have shown the existence of indirect pathways for both reactions (2) and (3); i. e., H_2 + O_2 → H + HO_2 → H_2O + O → 2OH. In symmetry restricted searches where only geometries possessing a plane (or more) of symmetry are considered, high lying "saddle points" can be located for both reactions (2) and (3). However, when the symmetry restriction is relaxed it is found that these are not true saddle points because they have two or more imaginary normal mode frequencies. The mode corresponding to one of the imaginary frequencies can be identified with reaction coordinates for reactions (2) or (3). The mode corresponding to one of the other imaginary frequency leads down to the transition state for (1). This suggests a potential energy landscape in which the H_2 + O_2 minimum is surrounded by a multi-dimensional ridge, the low point of which is the transition state for reaction (1). Thus, the picture that emerges from these calculations is that the lowest energy pathways for reactions (2) and (3) are step-wise processes in which the first step is reaction (1).

The final part of this theoretical treatment is a CTST calculation of the rate of reaction (1) using the unadjusted *ab initio* barrier height, structures, and frequencies given above. These calculations were carried out using the VARIFLEX program [38], within a rigid-rotor, harmonic oscillator approximation. Tunneling estimates were made using both Wigner and Eckart methods. The Wigner and Eckart tunneling estimates are found to be very similar, increasing the rate at 300°K by a factor of 3, while contributing only 10% at 1000°K and less than 1% at 2000°K. Both the experimental (points) and the theoretical (line) results of the present study are shown in Fig. 2 as an Arrhenius plot. The theoretical line in the figure can be expressed to within ±2% by the three-parameter equation:

$$k_1^{th} = 1.228 \times 10^{-18} T^{2.4328} \exp(-26926\ \mathrm{K/T})\ \mathrm{cm^3\ molecule^{-1}\ s^{-1}}, \qquad (8)$$

over the temperature range, 400-2300 K. Experimental data from previous work [7-10,13] on the reverse reaction (-1) have been transformed from k_{-1} to k_1 using the revised K_{eq}, Eq.

7. The completely *ab initio* result summarized by Eq. 8 is in excellent agreement with experiment over the entire T-range.

Conclusion: On both experimental and theoretical grounds, we therefore conclude that reactions (2) and (3) can be ignored and that only reaction (1) initiates chain branching in the H_2/O_2 system. The theoretical prediction of the rate behavior derived from first principles is in excellent agreement with experiment. We therefore recommend that the theoretical result, Eq. 8, should be exclusively used in modeling the branching chain oxidation of H_2. The remaining question to be answered is then whether this k_1 value can supply sufficient O-atom rates for the branching chain oxidation to occur. As is well known, ignition delay type experiments have traditionally monitored OH-radical production [22,39-48]. Using the mechanism of Table 2 along with Eq. 8, we simulated typical oxidation experiments at three temperatures. These simulations are shown in Fig. 3, and, in all cases, chain branching was clearly demonstrated. The experimental conditions for the 1927 K simulation are from this laboratory [48], and it is worth noting that the present simulation reproduces the experimental data shown in Fig. 4 of this earlier study. Even at 1300 K, rates of H and HO_2 formation calculated from Eq. 8 are large enough to initiate branching chain oxidation, although requiring a considerably longer induction time. Hence, we conclude that reaction (1) is the only important initiation process needed to explain H_2 oxidation by O_2.

Acknowledgments: This work was supported by the U. S. Department of Energy, Office of Basic Energy Sciences, Division of Chemical Sciences, under Contract No. W-31-109-Eng-38.

References

1. Semenov, N. , *Acta Physicochim. U. R. S. S.* 20:291-302 (1945).
2. Bradley, J. N., *Shock Waves in Chemistry and Physics*, Wiley, New York, 1962, p. 307.
3. Ripley, D. L. and W. C. Gardiner, Jr., *J. Chem. Phys.* 44:2285-2296 (1966).
4. Belles, F. E. and Brabbs, T. A., *Thirteenth Symposium (International) on Combustion*, the Combustion Institute, Pittsburgh, 1971, pp. 165-174.
5. Jachimowski, C. J. and Houghton, W. M., *Combust. and Flame*, 17:25-30 (1971).
6. Pamidimukkala, K. M. and Skinner, G. B., *Thirteenth International Symposium on Shock Waves and Shock Tubes,* State University of New York, Albany,1981, pp. 585-592.
7. Sridharan, U. C., Qui, L. X., and Kaufman, F., *J. Phys. Chem.* 86:4569-4574 (1982).
8. Keyser, L. F., *J. Phys. Chem.* 90:2994-3003 (1986).
9. Hack, W., Preuss, A. W., Wagner, H. Gg., and Hoyermann, K., *Ber. Bunsenges. Phys. Chem.* 83:212-217 (1979).
10. Thrush, B. A. and Wilkinson, J. P. T., *Chem. Phys. Lett.* 84:17-19 (1981).
11. Chase, M. W., Jr., Davies, C. A., Downey, J. R., Jr., Frurip, D. J., McDonald, R. A., and Syverud, A. N., *J. Phys. Chem. Ref. Data*14:Supplement No. 1 (1985).
12. Warnatz, J., In *Combustion Chemistry*, Gardiner, W. C. Jr., Ed., Springer, Heidelberg, 1984, p. 197.
13. Baldwin, R. R. and Walker, R. W., *Seventeenth Symposium (International) on Combustion*, the Combustion Institute, Pittsburgh, 1979, pp. 525-532; Baldwin, R. R., Fuller, M. E., Hillman, J. S., Jackson, D., and Walker, R. W., *J. Chem. Soc. Faraday Trans. 1* 70:635-641 (1974).
14. Tsang, W. and Hampson, R. F., *J. Phys. Chem. Ref. Data* 15:1087-1279 (1986).
15. Frank, P. and Just, Th., *Ber. Bunsenges. Phys. Chem.* 89:181-187 (1985).
16. Koike, T., *Bull. Chem. Soc. Jpn.* 62:2480-2483 (1989).
17. Michael, J. V., *J. Chem. Phys.* 90:189-198 (1989).
18. Michael, J. V. and Sutherland, J. W., *Int. J. Chem. Kinet.* 18:409-436 (1986).
19. Michael, J. V. and Lim, K. P., *J. Chem. Phys.* 97:3228-3234 (1992).
20. Maki, R. G.; Michael, J. V., and Sutherland, J. W. *J. Phys. Chem.* 89:4815-4821 (1985).

21. Michael, J. V., Kumaran, S. S., and Su, M.-C. *J. Phys. Chem.* 103:5942-5948 (1999).
22. Du, H. and Hessler, J. P., *J. Chem. Phys.* 96:1077-1092 (1992).
23. Michael, J. V., Kumaran, S. S., Su, M.-C., and Lim, K. P., *Science*, submitted.
24. Jerig, L., Thielen, K., and Roth, P., *AIAA J.* 29:1136-1139 (1991).
25. Michael, J. V., *Prog. Energy Combust. Sci.* 18:327-347 (1992).
26. Mallard, W. G.; Westley, F.; Herron, J. T.; Hampson, R. F. *NIST Chemical Kinetics Database – Ver. 6.0*, NIST Standard Reference Data, Gaithersburg, MD (1994).
27. Benson, S. W., *Thermochemical Kinetics*, 2nd Ed., Wiley, 1976.
28. Skinner, G. B., Lifshitz, A., Scheller, K., and Burcat. A., *J. Chem. Phys.* 56:3853-3861 (1972).
29. Dunning, T. H., Jr., *J. Chem. Phys.* 90:1007-1023 (1989).
30. Kendall, R.A., Dunning, T.H., Jr., and Harrison, R.J., *J. Chem. Phys.* 96:6796-6806 (1992).
31. Woon, D.E. and Dunning, T.H., Jr., *J. Chem. Phys.* 98:1358-1371 (1993).
32. Hampel, C., Peterson, K., and Werner, H.-J., *Chem. Phys. Lett.* 190:1-12 (1992), and references therein.
33. Werner, H.-J. and Knowles, P. J., *J. Chem. Phys.* 82:5053-5063 (1985).
34. Knowles, P. J. and Werner, H.-J., *Chem. Phys. Lett.* 115:259-267 (1985).
35. Werner, H.-J. and Knowles, P. J., with contributions from Almlof, J., Amos, R. D., Berning, A., Cooper, D. L., Deegan, M. J. O., Dobbyn, A. J., Eckert, F., Elbert, S. T., Hampel, C., Lindh, R., Lloyd, A. W., Meyer, W., Nicklass, A., Peterson, K., Pitzer, R., Stone, A. J., Taylor, P. R., Mura, M. E., Pulay, P., Schutz, M., Stoll, H., and Thorsteinsson, T., *MOLPRO*, http://www.tc.bham.ac.uk/molpro/; MOLPRO is a package of *ab initio* programs.
36. Litorja, M. and Ruscic, B., *J. Eletron Spectrosc.* 97:131-146 (1998).
37. Harding, L. B., In *Advances in Molecular Electronic Structure Theory*, Dunning, T. H., Jr., Ed., JAI Press, Greenwich, CT, 1990, p. 45.
38. Klippenstein, S. J., Wagner, A. F., Robertson, S. H., Dunbar, R. C., and Wardlaw, D. M., *VARIFLEX-version 1.0*, http://chemistry.anl.gov/variflex. VARIFLEX is a freeware program package for calculating gas phase reaction rates.

39. Bird, P. F. and Schott, G. L., *J. Quant. Spectrosc. Radiat. Transfer* 5:783-811 (1965); Schott, G. L. and Getzinger, R. W., In *Physical Chemistry of Fast Reactions*, (Levitt, P. B., Ed.), Plenum, London, 1973, p. 81, and references cited therein.
40. Bradley, J. N., Capey, W. D., Fair, R. W., and Pritchard, D. K., *Int. J. Chem. Kinet.* 8:549-561 (1976).
41. Jachimowski, C. J. and Houghton, W. M., *Combust. and Flame*, 15:125-132 (1970).
42. Gardiner, W. C., Jr., Mallard, W. G., and Owen, J. H., *J. Chem. Phys.* 60:2290-2295 (1974).
43. (a) Ernst, J., Wagner, H. Gg., and Zellner, R., *Ber. Bunsenges. Phys Chem.* 81:1270-1275 (1977); (b) Ernst, J., Wagner, H. Gg., and Zellner, R., *Ber. Bunsenges. Phys Chem.* 82:409-414 (1978); (c) Niemitz, K. J.,Wagner, H. Gg., and Zellner, R., *Z. Phys. Chemie* NF124:155-170 (1981).
44. (a) Hanson, R. K., Salimian, S., Kychankoff, G., and Booman, R. A., *Appl. Optics* 21: 641-643 (1983); (b) Rea, E. C., Jr., Chang, A. Y., and Hanson, R. K. *J. Quant. Spectrosc. Radiat. Transfer* 37:117-127 (1987); (c) Masten, D. A., Hanson, R. K., and Bowman, C. T., *J. Phys. Chem.* 94:7119-7128 (1990).
45. Yuan, T., Wang, C., Yu, C.-L., Frenklach, M., and Rabinowitz, M. J., *J. Phys. Chem.* 95:1258-1265 (1991).
46. (a) Fujii, N. and Shin, K. S. *Chem. Phys. Lett.* 151:461-465 (1988); (b) Yang, H., Gardiner, W. C., Jr., Shin, K. S., and Fujii, N., *Chem. Phys. Lett.* 231:449-453 (1994).
47. (a) Ryu, S.-O., Hwang, S. M., and Rabinowitz, M. J., *Chem. Phys. Lett.* 242:279-284 (1995); (b)) Ryu, S.-O., Hwang, S. M., and Rabinowitz, M. J., *J. Phys. Chem.* 99:13984-13991 (1995).
48. Su., M.-C., Kumaran, S. S., Lim, K. P., and Michael, J. V., *Rev. Sci. Inst.* 66:4649-4654 (1995).

Table 1: High Temperature Rate Data for $H_2 + O_2$

P_1 / Torr	M_s[a]	ρ_5 / (10^{18} cm^{-3})[b]	T_5 / K[b]	k_1 /(cm^3 s^{-1})[c]
	$X_{H_2} = 2.494 \times 10^{-5}$		$X_{O_2} = 6.123 \times 10^{-2}$	
10.91	3.013	2.620	2097	3.0(-16)[d]
10.96	2.877	2.532	1927	9.0(-17)
10.93	2.853	2.508	1897	9.0(-17)
10.92	2.861	2.511	1907	2.0(-16)
10.94	2.806	2.466	1848	1.0(-16)
10.94	2.981	2.596	2063	2.5(-16)
10.94	2.915	2.549	1981	1.6(-16)
10.97	2.793	2.470	1826	1.0(-16)
10.91	2.904	2.542	1960	1.0(-16)
	$X_{H_2} = 5.023 \times 10^{-5}$		$X_{O_2} = 6.177 \times 10^{-2}$	
10.91	2.783	2.442	1819	3.2(-17)
10.92	2.810	2.465	1851	3.0(-17)
10.93	2.843	2.493	1891	1.1(-16)
10.94	2.775	2.442	1810	8.0(-17)
10.99	2.668	2.373	1679	5.0(-17)
10.89	2.889	2.519	1948	1.5(-16)
10.93	2.910	2.544	1974	1.1(-16)
10.93	2.901	2.538	1963	1.3(-16)
10.91	2.938	2.568	2002	1.4 (-16)
	$X_{H_2} = 7.468 \times 10^{-5}$		$X_{O_2} = 6.122 \times 10^{-2}$	
10.91	2.834	2.481	1881	8.0(-17)
10.91	2.803	2.456	1844	9.0(-17)
10.97	2.678	2.368	1698	1.5(-17)
10.92	2.798	2.455	1838	4.2(-17)
10.89	2.782	2.436	1819	2.6(-17)
10.93	2.753	2.421	1785	2.0(-17)
10.92	2.647	2.331	1662	1.6(-17)
10.92	2.684	2.362	1704	1.5(-17)
10.88	2.896	2.529	1950	9.0(-17)
10.93	2.785	2.447	1822	4.0(-17)

---

[a] The error in measuring the Mach number, M_S, is typically 0.5-1.0 % at the one standard deviation level. [b] Quantities with the subscript 5 refer to the thermodynamic state of the gas in the reflected shock region. [c] Fitted rate constants for reaction (1) (see text). [d] Parentheses denotes the power of 10.

Table 2: Mechanism used for fitting [O] profiles from $H_2 + O_2$.[a]

1.	$H_2 + O_2 \rightarrow H + HO_2$	k_1 = fitted
2.	$H_2 + O_2 \rightarrow OH + OH$	$k_2 = 0$
3.	$H_2 + O_2 \rightarrow O + H_2O$	$k_3 = 0$
4.	$H_2 + Kr \rightarrow H + H + Kr$	$k_4 = 8.86 \times 10^{-10} \exp(-48321\ K/T)$ [b]
5.	$O_2 + Kr \rightarrow O + O + Kr$	$k_5 = 2.66 \times 10^{-6}\ T^{-1} \exp(-59380\ K/T)$ [c]
6.	$H + O_2 \rightarrow OH + O$	$k_6 = 1.62 \times 10^{-10} \exp(-7474\ K/T)$ [d]
7.	$HO_2 + Kr \rightarrow H + O_2 + Kr$	$k_7 = 2.0 \times 10^{-5}\ T^{-1.18} \exp(-24363\ K/T)$ [e]
8.	$OH + H_2 \rightarrow H_2O + H$	$k_8 = 3.56 \times 10^{-16}\ T^{1.52} \exp(-1736\ K/T)$ [d]
9.	$O + H_2 \rightarrow OH + H$	$k_9 = 8.44 \times 10^{-20}\ T^{2.67} \exp(-3167\ K/T)$ [d]
10.	$OH + OH \rightarrow O + H_2O$	$k_{10} = 7.19 \times 10^{-21}\ T^{2.7} \exp(1251\ K/T)$ [d]
11.	$OH + O \rightarrow O_2 + H$	$k_{11} = 5.42 \times 10^{-13}\ T^{0.375} \exp(1112\ K/T)$ [d]
12.	$H + H_2O \rightarrow OH + H_2$	$k_{12} = 1.56 \times 10^{-15}\ T^{1.52} \exp(-9249\ K/T)$ [d]
13.	$O + H_2O \rightarrow OH + OH$	$k_{13} = 7.48 \times 10^{-20}\ T^{2.7} \exp(-7323\ K/T)$ [d]
14.	$H + HO_2 \rightarrow H_2 + O_2$	$k_{14} = k_1/K_{eq}$ [f]
15.	$H + OH \rightarrow H_2 + O_2$	$k_{15} = 3.78 \times 10^{-20}\ T^{2.67} \exp(-2226\ K/T)$ [d]

---

[a] All rate constants are in $cm^3\ molecule^{-1}\ s^{-1}$. [b] Refs. 22, 23. [c] Ref. 24. [d] Ref. 25. [e] Refs. 14, 26. [f] Calculated from Eq. 7.

Figure Captions

Fig. 1 Comparison of measured and simulated O-atom profiles for initiation by reaction (1), ——, or reaction (2), – – –. Top panel: $P_1 = 10.94$ Torr, $M_s = 2.915$, $\rho_5 = 2.549 \times 10^{18}$, $T_5 = 1981$ K, $[H_2] = 6.357 \times 10^{13}$, and $[O_2] = 1.561 \times 10^{17}$, all in molecules cm^{-3}, $k_1 = 1.6 \times 10^{-16}$ cm^3 molecule^{-1} s^{-1} or $k_2 = 7.3 \times 10^{-16}$ cm^3 molecule^{-1} s^{-1}. Bottom panel: $P_1 = 10.94$ Torr, $M_s = 2.775$, $\rho_5 = 2.442 \times 10^{18}$, $T_5 = 1810$ K, $[H_2] = 1.227 \times 10^{14}$, and $[O_2] = 1.508 \times 10^{17}$, all in molecules cm^{-3}, $k_1 = 8.0 \times 10^{-17}$ cm^3 molecule^{-1} s^{-1} or $k_2 = 2.25 \times 10^{-16}$ cm^3 molecule^{-1} s^{-1}.

Fig. 2 Arrhenius plot of the data for k_1. ○ — data from Table 1. The line is the *ab initio* theoretical calculation summarized by the three parameter expression, Eq. 8. ■ — data of ref. 13 and ● — data of refs. 7-10, both transformed using Eq. 7. Insert: ○ — data from Table 1. The line is the theoretical calculation summarized by Eq. 8.

Fig. 3 A simulation of OH profiles at three temperatures (from left to right, 1927, 1700, and 1390 K, respectively), using the mechanism of Table 2 with the theoretical value for k_1 as given by Eq. 8. $[H_2] = 6.524 \times 10^{16}$ and $[O_2] = 6.522 \times 10^{15}$, both in molecules cm^{-3} for all three simulations. The simulation at 1927 K reproduces the experimental data reported in ref. 48.

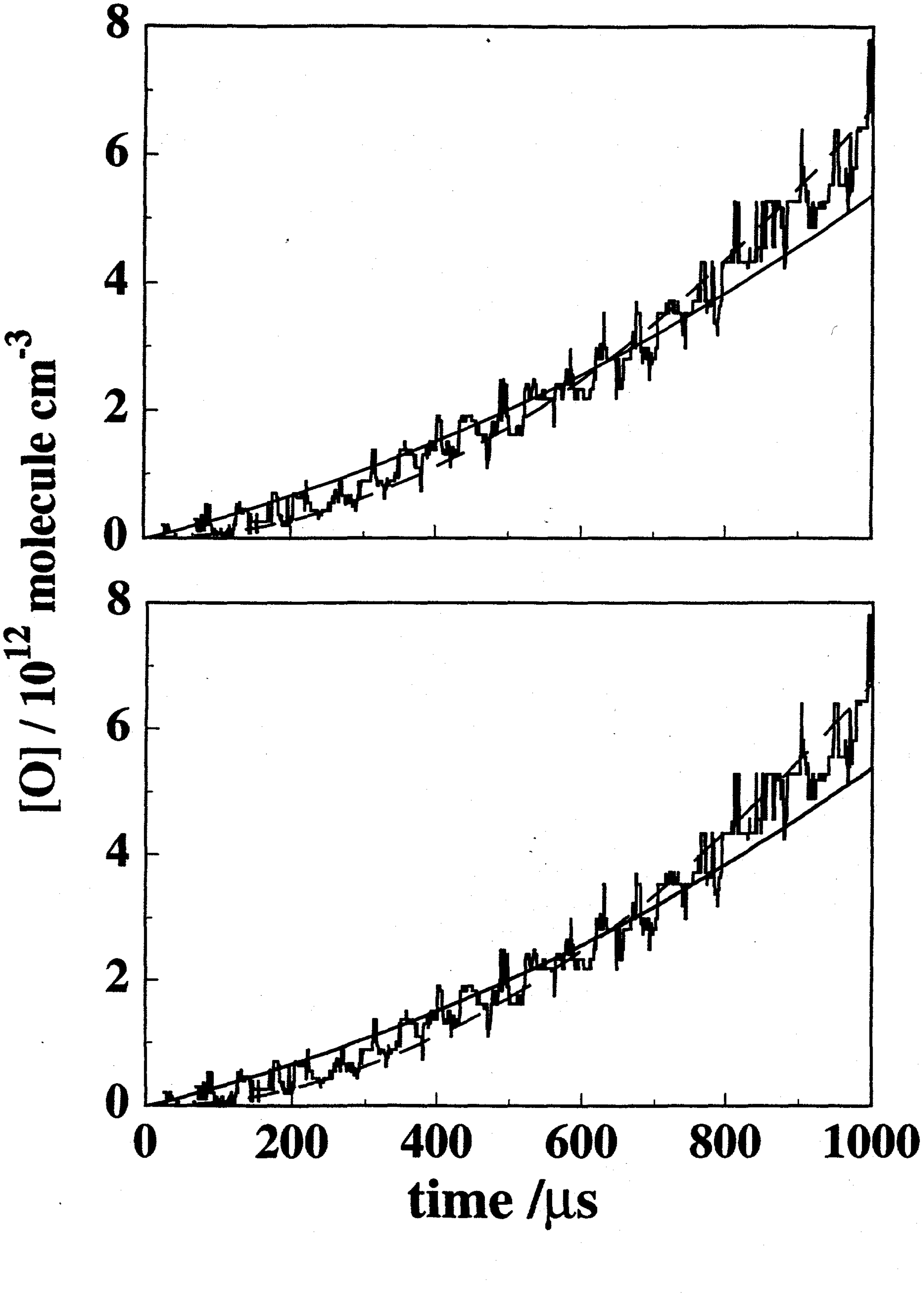

8
6
4
2
0
8
6
4
2
0
0
200
400
600
800
1000
time /μs
[O] / 10^{12} molecule cm^{-3}

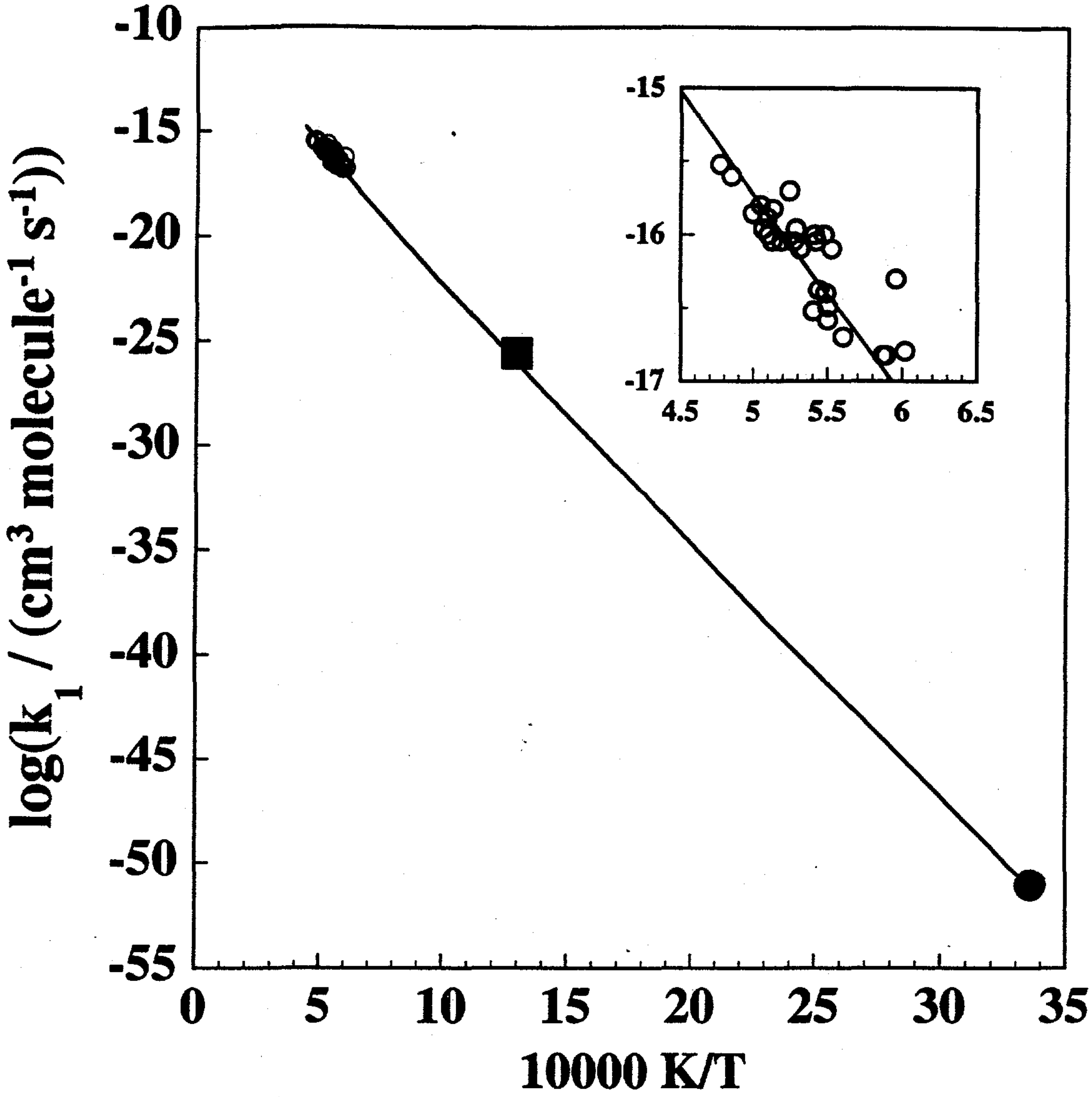
log(k$_1$ / (cm^3 molecule^{-1} s^{-1}))
10000 K/T
-10
-15
-20
-25
-30
-35
-40
-45
-50
-55
0
5
10
15
20
25
30
35
-15
-16
-17
4.5
5
5.5
6
6.5

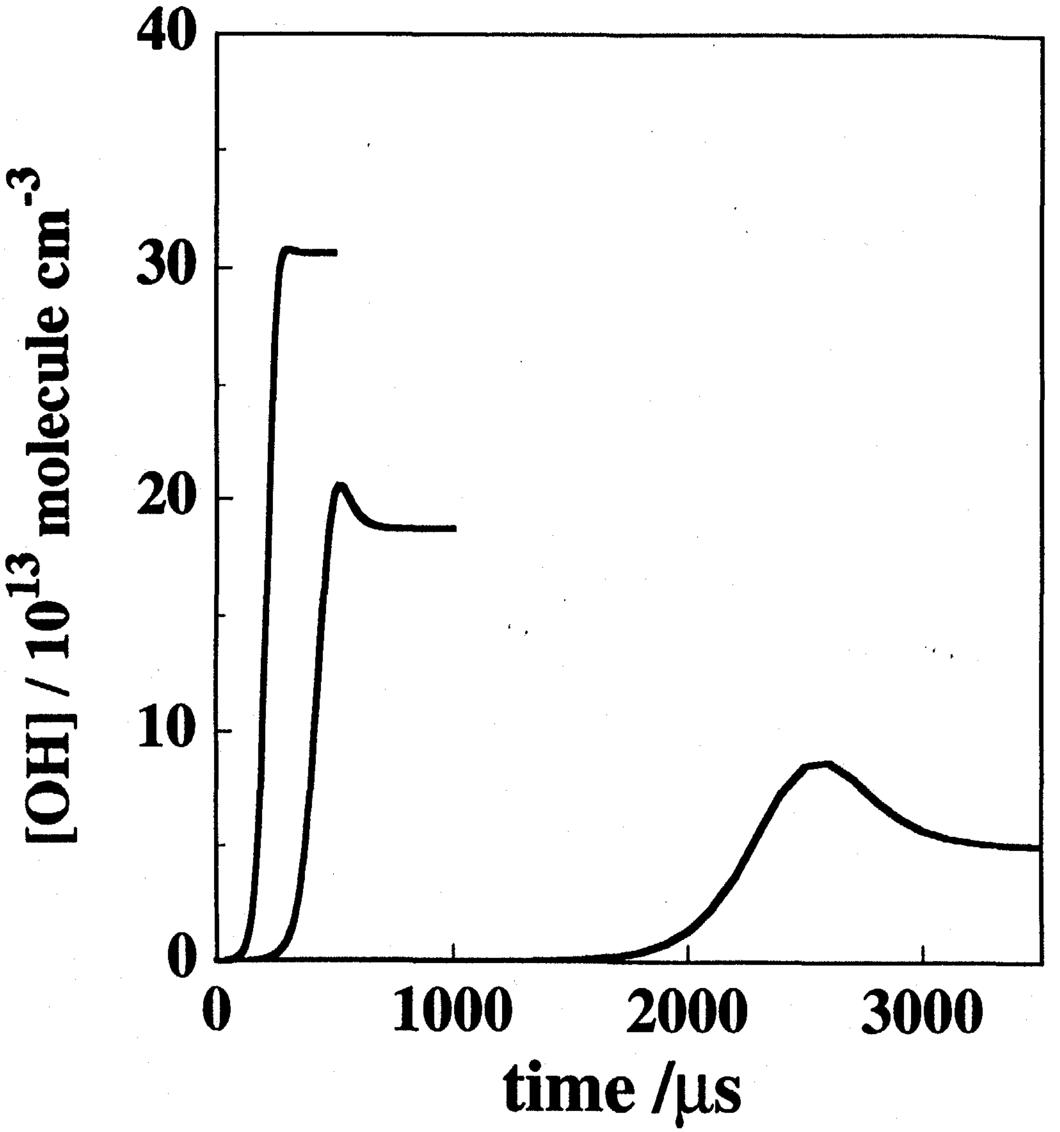

40
30
20
10
0
[OH] / 10^13 molecule cm^-3
0
1000
2000
3000
time /μs